Journal of Systems Engineering and Electronics
Vol. 32, No. 1, February 2021, pp.81 – 91

SAR image de-noising via grouping-based PCA and guided filter

FANG Jing[1,2,*], HU Shaohai[1,*], and MA Xiaole[1]

1. Institute of Information Science, Beijing Jiaotong University, Beijing 100044, China; 2. Shandong Province Key Laboratory of Medical Physics and Image Processing Technology, School of Physics and Electronics, Shandong Normal University, Jinan 250014, China

Abstract: A novel synthetic aperture radar (SAR) image de-noising method based on the local pixel grouping (LPG) principal component analysis (PCA) and guided filter is proposed. This method contains two steps. In the first step, we process the noisy image by coarse filters, which can suppress the speckle effectively. The original SAR image is transformed into the additive noise model by logarithmic transform with deviation correction. Then, we use the pixel and its nearest neighbors as a vector to select training samples from the local window by LPG based on the block similar matching. The LPG method ensures that only the similar sample patches are used in the local statistical calculation of PCA transform estimation, so that the local features of the image can be well preserved after coefficients shrinkage in the PCA domain. In the second step, we do the guided filtering which can effectively eliminate small artifacts left over from the coarse filtering. Experimental results of simulated and real SAR images show that the proposed method outstrips the state-of-the-art image de-noising methods in the peak signal-to-noise ratio (PSNR), the structural similarity (SSIM) index and the equivalent number of looks (ENLs), and is of perceived image quality.

Keywords: synthetic aperture radar (SAR) image de-noising, local pixel grouping (LPG), principal component analysis (PCA), guided filter.

DOI: 10.23919/JSEE.2021.000009

1. Introduction

Synthetic aperture radar (SAR) remote sensing has many advantages compared with optical remote sensing, mainly the capture ability of all-day and all-weather [1]. However, the main drawback of SAR images is the existence of speckle noise, which is a kind of signal related particle noise called speckle noise. Speckle noise can affect the subsequent image interpretation and information extraction [2−4].

Manuscript received March 12, 2018.
*Corresponding author.
This work was supported by the National Natural Science Foundation of China (62002208; 61572063; 61603225), and the Natural Science Foundation of Shandong Province (ZR2016FQ04).

During the past three decades, several SAR image de-noising methods have been proposed. Many scholars take a great loss of image resolution as the cost and average a certain number of independent images to solve this problem. Some of the early speckle reduction techniques are based on the logarithmic transformation to obtain an additive model which is easier to deal with. Then some famous methods to de-noise the additive white Gaussian noise (AWGN) can be used as a reference to deal with the transformed model [5,6]. These methods often neglect some basic properties of the speckles although they are easy to implement. In practical terms, the log-transformed speckle noise does not strictly obey the zero mean Gaussian distribution. Therefore, the deviation needs to be corrected before any other processing is carried out [7]. In the corresponding period, more ambitious techniques tackle de-noising in the original domain based on the multiplicative speckle model. These early articles have clearly shown that some form of local adaptation is needed to account for the nonstationarity of the image [8−11]. With the development and continuous improvement of the multi-scale analysis tool, there are more and more techniques tackling de-noising in the transform domain. After a homomorphic transformation, wavelet shrinkage can be readily applied to the transformed coefficients. As well as the spatial domain, the wavelet-based techniques take some advantages of spatial adaptivity when filtering the image so as to better retain image textures and boundaries [12−16].

The nonlocal means (NLM) methods as a brand-new image de-noising strategy were proposed in recent years [17−24]. The basic idea is to use the self-similarity of natural images. The NLM methods have been used in SAR image de-noising. Among them the most famous algorithms are the probabilistic patch-based (PPB) algorithm [18] and the SAR block matching 3D (SAR-BM3D) algorithm [21]. In recent years, the convolutional neural networks have been developed rapidly and play an impor-

tant role in Gaussian noise filtering which have been extended to SAR images de-noising [25,26]. Nevertheless, it can be a time-consuming operation to train these networks and set up a training set with pairs of speckle-free SAR images.

In this paper, we go one step further and propose a semi-non-local principal component analysis (PCA)-based de-noising method for SAR images. The PCA is a classical de-correlation technology in statistical signal processing which is widely used in pattern recognition and dimensionality reduction and other fields [27]. In the PCA domain, the principal components (PCs) represent the scene information, while the last secondary components mainly represent the noise information [28]. The adaptive PCA de-noising method proposed by Muresan and Parks [29] and the local pixel grouping PCA (LPG-PCA) method proposed by Zhang et al. [30] all adopt linear minimum mean-square error (LMMSE) to shrink the PCA transform coefficients, so as to achieve the purpose of filtering Gaussian noise. Both methods are more effective than the traditional wavelet-based de-noising methods.

Aiming at the multiplicative nature of speckle noise, a new de-noising strategy based on the LPG-PCA technology is established in this paper. Considering the particularity of the SAR image in the original domain, we construct the pixel to be processed and its nearest neighbors as a vector. Inspired by [21], we select the training samples by an ad hoc measure and obtain the vectors of similar image patches. Through similarity grouping, the local statistical information of the SAR image can be better calculated. Thus, the edge information of the scene can be better protected when the PCA transform coefficients are shrunk. However, there may be the wrong grouping caused by strong noise. We use the guided filter as a good contour preserving strategy to improve the de-noising results [31,32].

The rest of this paper is arranged as follows. Section 2 reviews the data formation and statistics of SAR images after logarithmic transformation based on the PCA. Section 3 introduces the SAR image de-noising method based on the LPG-PCA. Section 4 recommends the guided filter. Section 5 describes the proposed method. Section 6 shows the results obtained by using both simulated and real SAR images. Finally, in Section 7, we make a conclusion.

2. SAR image statistics and PCA

In this section, two important preprocessing steps are introduced that will run through this article. First we review the logarithmic SAR statistics and get the mean and variance of the log-transformed model. Then, we briefly review the procedure of the PCA.

2.1 SAR image statistics

SAR remote sensing is an active acquisition device which transmits radar signals and captures the reflected echoes from the in-phase and quadrature channels. The received echoes are very difficult to analyze. Due to the unevenness of the reflector, the interference will occur in each resolution cell. As a result, light and dark particles will inevitably appear in SAR images called speckle noise.

Assuming that the speckle noise is fully developed, the received reflected signal model can be denoted by

$$\boldsymbol{I} = \boldsymbol{R}\boldsymbol{V} \tag{1}$$

where $\boldsymbol{I}$ denotes the observed noise image, $\boldsymbol{R}$ represents the noise-free reflected signal which is an auto-correlated random process, and $\boldsymbol{V}$ is the speckle fading term which obeys auto-correlation stationary random distribution. The model represented by (1) is suitable for single-look or multi-look images and the quantities can be amplitude or intensity. Goodman [2] proved that fully developed speckle follows the Gamma distribution. In a homogeneous region, the equivalent number of looks (ENLs) is often regarded as a known parameter which can be calculated as

$$L = \frac{\mu^2}{\sigma^2} \tag{2}$$

where μ denotes the mean value and σ denotes the standard deviation of the homogeneous region.

Since the observed signal and the noise-free signal are nonlinear, it is a very difficult task to filter the SAR speckle noise. The multiplicative noise model is transformed into the additive noise model by logarithmic transformation, i.e.,

$$\ln(\boldsymbol{I}) = \ln(\boldsymbol{R}) + \ln(\boldsymbol{V}). \tag{3}$$

The mean of $\ln(\boldsymbol{V})$ can be calculated by the following formula:

$$\mathrm{E}[\ln(\boldsymbol{V})] = \psi^{(0)}(L) - \ln(L), \tag{4}$$

and the variance also can be denoted by

$$\mathrm{var}[\ln(\boldsymbol{V})] = \psi^{(1)}(L) \tag{5}$$

where $\psi^{(m)}(L)$ is the Poly-Gamma function with order m [7]. The model after logarithmic transformation does not strictly obey the Gaussian distribution with zero mean. It is necessary to correct the deviation, so the observed signal can be denoted by

$$\boldsymbol{I}^{(\ln)} = \ln(\boldsymbol{I}) - \psi^{(0)}(L) + \ln(L). \tag{6}$$

In the following research, we will start from the above model and further assume that the signal and noise are not spatially correlated. Firstly, the PCA is introduced.

2.2 PCA

Let $\boldsymbol{x}=[x_1,x_2,\cdots,x_m]^{\mathrm{T}}$ be a vector variable with m components and

$$\boldsymbol{X}=\begin{bmatrix} x_1^{(1)} & x_1^{(2)} & \cdots & x_1^{(n)} \\ x_2^{(1)} & x_2^{(2)} & \cdots & x_2^{(n)} \\ \vdots & \vdots & \ddots & \vdots \\ x_m^{(1)} & x_m^{(2)} & \cdots & x_m^{(n)} \end{bmatrix} \tag{7}$$

be the sample matrix of $\boldsymbol{x}$, where $x_i^{(j)}$ are the samples of variable x_i, $i=1,2,\cdots,m$, and $j=1,2,\cdots,n$. The sample vector $\boldsymbol{X}_i$ is the ith row vector of sample matrix $\boldsymbol{X}$ which includes n elements denoted by

$$\boldsymbol{X}_i=\left[\ x_i^{(1)},\ x_i^{(2)},\ \cdots,\ x_i^{(n)}\ \right]. \tag{8}$$

We can calculate the mean value of $\boldsymbol{X}_i$ as

$$\mu_i=\frac{1}{n}\sum_{j=1}^{n}x_i^{(j)}. \tag{9}$$

The sample vector $\boldsymbol{X}_i$ is centralized as

$$\bar{\boldsymbol{X}}_i=\boldsymbol{X}_i-\mu_i=\left[\bar{x}_i^{(1)},\bar{x}_i^{(2)},\cdots,\bar{x}_i^{(n)}\right] \tag{10}$$

where $\bar{x}_i^{(j)}=x_i^{(j)}-\mu_i$. Therefore, the sample matrix $\boldsymbol{X}$ can be centralized as

$$\bar{\boldsymbol{X}}=\left[\bar{\boldsymbol{X}}_1^{\mathrm{T}},\bar{\boldsymbol{X}}_2^{\mathrm{T}},\cdots,\bar{\boldsymbol{X}}_m^{\mathrm{T}}\right]^{\mathrm{T}}. \tag{11}$$

Finally, we can calculate the co-variance matrix of $\bar{\boldsymbol{X}}$ as

$$\boldsymbol{\Omega}=\frac{1}{n}\bar{\boldsymbol{X}}\bar{\boldsymbol{X}}^{\mathrm{T}}. \tag{12}$$

Let $\boldsymbol{\Phi}=\left[\ \varphi_1,\varphi_2,\cdots,\varphi_m\ \right]$ be the $m\times m$ orthonormal eigenvector matrix of $\boldsymbol{\Omega}$, and $\boldsymbol{\Lambda}=\mathrm{diag}\{\lambda_1,\lambda_2,\cdots,\lambda_m\}$ be the diagonal eigenvalue matrix. The covariance matrix, as we all know, is symmetrical, which can be decomposed into

$$\boldsymbol{\Omega}=\boldsymbol{\Phi}\boldsymbol{\Lambda}\boldsymbol{\Phi}^{\mathrm{T}}. \tag{13}$$

The terms $\varphi_1,\varphi_2,\cdots,\varphi_m$ and $\lambda_1,\lambda_2,\cdots,\lambda_m$ are the eigenvectors and eigenvalues of $\boldsymbol{\Omega}$ respectively. Meanwhile the eigenvalues are in the non-increasing order. The purpose of PCA transformation is to find the orthonormal transformation matrix to de-correlate the data matrix. By setting

$$\boldsymbol{P}=\boldsymbol{\Phi}^{\mathrm{T}}\bar{\boldsymbol{X}}, \tag{14}$$

$\bar{\boldsymbol{X}}$ can be de-correlated. The PCA transformation may completely de-correlate the original dataset $\bar{\boldsymbol{X}}$. In the PCA domain, the energy of signals concentrates on a small subset, while the energy of noise will evenly distribute over the whole dataset. Therefore, the small coefficients in the PCA domain can be considered as noise signals which should be shrunk.

3. SAR image de-noising by LPG-PCA

In Section 3, based on the aforementioned model and the de-correlation between the signal and the noise in the log-transform domain, we will first introduce the local pixel grouping and the block similarity measure (BSM) applying to the SAR image.

The size of the SAR image is usually very large. It often ignores weak patterns when grouping the image pixels directly. Therefore, we divide the large image into several training blocks and get the training samples. Suppose there is a $K\times K$ training block as shown in Fig. 1. We model the central pixel to be de-noised and its nearest neighbors as a vector. An $N\times N$ window centered on the pixel is shown in Fig. 1. Obviously there are N^2 elements in the window, which is defined as $\boldsymbol{x}=[x_1,x_2,\cdots,x_m]^{\mathrm{T}}$, $m=N^2$. We perform the noise removal on the obtained vector, rather than on the single pixel in the center of the window.

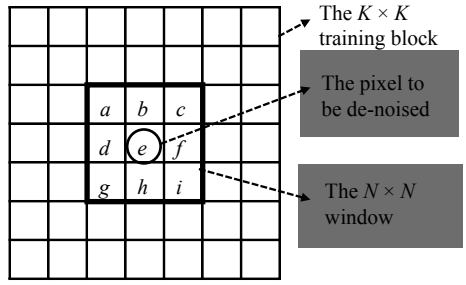

Fig. 1 Schematic diagram of local-pixel-grouping

According to the additive noise model discussed in Section 2, the patch variable in the training block can be denoted by

$$\boldsymbol{y}=\boldsymbol{x}+\boldsymbol{u} \tag{15}$$

where $\boldsymbol{y}=[y_1,y_2,\cdots,y_m]^{\mathrm{T}}$, $\boldsymbol{u}=[u_1,u_2,\cdots,u_m]^{\mathrm{T}}$ and $y_k=x_k+u_k$ $(k=1,2,\cdots,m)$. In order to recover $\boldsymbol{x}$ from $\boldsymbol{y}$ more effectively, we regard $\boldsymbol{x}$ and $\boldsymbol{y}$ as noiseless and noisy vectors respectively. In order to carry out the PCA transformation, we need to find a set of training samples of $\boldsymbol{y}$. The classical PCA transformation goes through all the $N\times N$ patches in the $K\times K$ training window. Therefore, for each component y_k of $\boldsymbol{y}$, there are altogether $N^{(p)}=(K-N+1)^2$ training samples. However, the effectiveness of the de-noising method by the PCA depends on whether the principal components can represent the scene signal sparsely. In view of this, we may perform the analysis on similar patches to get sparser representation. Therefore, it is necessary to select the similar samples based on

the spatial information and group the training samples before the PCA transformation.

3.1 LPG in SAR images

The similarity between vectors is usually inversely proportional to some distance measure. Therefore, the smaller the distance is, the higher the similarity becomes. There are different approaches to look for the similar patches, such as K-means clustering, block matching, and l^p-norm. The original LPG-PCA algorithm utilizes the Euclidean distance as the similarity measurement between the patch vectors. Considering the distribution of actual speckle noise, it is not an appropriate choice for SAR images. Parrilli et al. [21] proposed an ad hoc BSM. In this paper, the BSM is used as the similarity measurement between different patches.

Let $\boldsymbol{y}_r$ be the "reference column vector" which contains all the pixels in the central $N\times N$ window. r denotes the pixel to be processed and k is used to scan the whole window. The other patches in the training block can be denoted by $\boldsymbol{y}_i$, where $i=1,\cdots,(K-N+1)^2-1$. Let $\boldsymbol{x}_r$ and $\boldsymbol{x}_i$ be the noiseless column sample vectors corresponding to $\boldsymbol{y}_r$ and $\boldsymbol{y}_i$, respectively.

Considering the SAR image model, we define the BSM as

$$d_1[\boldsymbol{y}_r,\boldsymbol{y}_i]=-\ln\left\{\prod_k p[\boldsymbol{y}(r+k),\boldsymbol{y}(i+k)]\,|\,\boldsymbol{x}(r+k)=\boldsymbol{x}(i+k)\right\}=-\ln\left\{\prod_k 4L\frac{\Gamma(2L-1)}{\Gamma^2(L)}\cdot\left[\frac{\boldsymbol{y}(r+k)\boldsymbol{y}(i+k)}{\boldsymbol{y}^2(r+k)+\boldsymbol{y}^2(i+k)}\right]^{2L-1}\right\} \tag{16}$$

where $\Gamma()$ is the Gamma function and L is the ENLs.

Equation (16) can be further simplified by the properties of logarithmic operation,

$$d_1[\boldsymbol{y}_r,\boldsymbol{y}_i]=-\ln\left[4L\frac{\Gamma(2L-1)}{\Gamma^2(L)}\right]-\sum_k\ln\left[\frac{\boldsymbol{y}(r+k)\boldsymbol{y}(i+k)}{\boldsymbol{y}^2(r+k)+\boldsymbol{y}^2(i+k)}\right]^{2L-1}=$$
$$-\ln\left[4L\frac{\Gamma(2L-1)}{\Gamma^2(L)}\right]+(2L-1)\sum_k\ln\left[\frac{\boldsymbol{y}^2(r+k)+\boldsymbol{y}^2(i+k)}{\boldsymbol{y}(r+k)\boldsymbol{y}(i+k)}\right]=$$
$$\ln\left[4L\frac{\Gamma(2L-1)}{\Gamma^2(L)}\right]+(2L-1)\sum_k\ln\left[\frac{\boldsymbol{y}(r+k)}{\boldsymbol{y}(i+k)}+\frac{\boldsymbol{y}(i+k)}{\boldsymbol{y}(r+k)}\right]. \tag{17}$$

The first term is constant which can be discarded. Thus the BSM can be represented as

$$d[\boldsymbol{y}_r,\boldsymbol{y}_i]=(2L-1)\sum_k\ln\left[\frac{\boldsymbol{y}(r+k)}{\boldsymbol{y}(i+k)}+\frac{\boldsymbol{y}(i+k)}{\boldsymbol{y}(r+k)}\right]. \tag{18}$$

If d-distance follows (19), we consider $\boldsymbol{y}_i$ the similar sample vector of $\boldsymbol{y}_r$,

$$d[\boldsymbol{y}_r,\boldsymbol{y}_i]\leqslant\tau_{\text{match}}^{\text{ht}} \tag{19}$$

where $\tau_{\text{match}}^{\text{ht}}$ is the maximum d-distance between two similar patches. Inspired by [30], we select the parameter $\tau_{\text{match}}^{\text{ht}}$ from the deterministic speculations about the acceptable value of the ideal difference, while ignore the noisy components of the observed signal.

Suppose n sample vectors of $\boldsymbol{y}$ have been selected, which can be written as $\boldsymbol{y}_r,\boldsymbol{y}_1,\boldsymbol{y}_2,\cdots,\boldsymbol{y}_{n-1}$. The corresponding noiseless vector can be denoted by $\boldsymbol{x}_r,\boldsymbol{x}_1,\boldsymbol{x}_2,\cdots,\boldsymbol{x}_{n-1}$. Then the training dataset for $\boldsymbol{y}$ is denoted by

$$\boldsymbol{Y}=[\boldsymbol{y}_r,\boldsymbol{y}_1,\boldsymbol{y}_2,\cdots,\boldsymbol{y}_{n-1}]. \tag{20}$$

The noiseless counterpart of $\boldsymbol{Y}$ is formed by

$$\boldsymbol{X}=[\boldsymbol{x}_r,\boldsymbol{x}_1,\boldsymbol{x}_2,\cdots,\boldsymbol{x}_{n-1}]. \tag{21}$$

In order to calculate the PCA transformation matrix more accurately, n should not be too small. In general, we select at least $c\cdot m$ similar samples from the training blocks, where c is a constant between 7 and 10 determined by experiments. That is to say, if $n<c\cdot m$, we will use the best $c\cdot m$ matched samples in PCA training. Generally, the most similar training samples can improve the robustness of local information estimation. The accuracy of the PCA transformation matrix can be improved by using local similarity grouping.

3.2 SAR image de-noising in the PCA domain

Next, we discuss how to recover the noiseless dataset $\boldsymbol{X}$ from the noisy measurement $\boldsymbol{Y}$.

In the $m\times n$ dataset matrix $\boldsymbol{Y}$, each component $\boldsymbol{y}_i$ of the vector $\boldsymbol{y}$ has n samples, where $i=1,2,\cdots,m$. Let $\boldsymbol{Y}_i$ be the row vector which contains n samples of $\boldsymbol{y}_i$. Thus the dataset $\boldsymbol{Y}$ can be denoted by $\boldsymbol{Y}=[\boldsymbol{Y}_1^{\mathrm{T}},\cdots,\boldsymbol{Y}_m^{\mathrm{T}}]^{\mathrm{T}}$.

Similarly, $\boldsymbol{X}=[\boldsymbol{X}_1^{\mathrm{T}},\cdots,\boldsymbol{X}_m^{\mathrm{T}}]^{\mathrm{T}}$ and $\boldsymbol{U}=[\boldsymbol{U}_1^{\mathrm{T}},\cdots,\boldsymbol{U}_m^{\mathrm{T}}]^{\mathrm{T}}$ represent the noiseless counterpart and the noise variable dataset respectively. Then $\boldsymbol{Y}_i$ is centralized by $\bar{\boldsymbol{Y}}_i=\boldsymbol{Y}_i-\mu_i$, where $\mu_i=\dfrac{1}{n}\sum_{j=1}^{n}\boldsymbol{Y}_i(j)$ is the mean value. Because the mean of the noise in (6) is zero, $\boldsymbol{X}_i$ can also be centralized by $\bar{\boldsymbol{X}}_i=\boldsymbol{X}_i-\mu_i$. Then we get the centralized datasets denoted by $\bar{\boldsymbol{Y}}=\left[\bar{\boldsymbol{Y}}_1^{\mathrm{T}},\cdots,\bar{\boldsymbol{Y}}_m^{\mathrm{T}}\right]^{\mathrm{T}}$ and $\bar{\boldsymbol{X}}=\left[\bar{\boldsymbol{X}}_1^{\mathrm{T}},\cdots,\bar{\boldsymbol{X}}_m^{\mathrm{T}}\right]^{\mathrm{T}}$. The centralized datasets also obey the additive model

$$\bar{\boldsymbol{Y}}=\bar{\boldsymbol{X}}+\boldsymbol{U}. \tag{22}$$

As we have discussed in Subsection 2.2, once the covariance matrix $\boldsymbol{\Omega}_{\bar{X}}$ is calculated, the PCA transformation matrix $\boldsymbol{P}_{\bar{X}}$ can be obtained. Instead, depressingly, the centralized dataset $\bar{\boldsymbol{Y}}$ is corrupted by the noise which makes it difficult to calculate the covariance matrix $\boldsymbol{\Omega}_{\bar{X}}$. In order to solve this problem, we first calculate the covariance matrix of $\bar{\boldsymbol{Y}}$, denoted by $\boldsymbol{\Omega}_{\bar{Y}}$. Carrying out singular value decomposition (SVD) on the covariance matrix $\boldsymbol{\Omega}_{\bar{Y}}$, we can obtain the PCA bases. That is,

$$\boldsymbol{\Omega}_{\bar{Y}} = \frac{1}{n}\bar{\boldsymbol{Y}}\bar{\boldsymbol{Y}}^{\mathrm{T}} = \frac{1}{n}(\bar{\boldsymbol{X}}\bar{\boldsymbol{X}}^{\mathrm{T}} + \bar{\boldsymbol{X}}\boldsymbol{U}^{\mathrm{T}} + \boldsymbol{U}\bar{\boldsymbol{X}}^{\mathrm{T}} + \boldsymbol{U}\boldsymbol{U}^{\mathrm{T}}) \approx \frac{1}{n}(\bar{\boldsymbol{X}}\bar{\boldsymbol{X}}^{\mathrm{T}} + \boldsymbol{U}\boldsymbol{U}^{\mathrm{T}}) = \boldsymbol{\Omega}_{\bar{X}} + \boldsymbol{\Omega}_{U}. \tag{23}$$

As described in [30], the eigenvector matrices of $\boldsymbol{\Omega}_{\bar{Y}}$ and $\boldsymbol{\Omega}_{\bar{X}}$ are the same. Thus in practical implementation we can perform SVD on $\boldsymbol{\Omega}_{\bar{Y}}$ to get the PCA bases,

$$\boldsymbol{\Omega}_{\bar{Y}} = \boldsymbol{\Phi}_{\bar{Y}}\boldsymbol{\Lambda}_{\bar{Y}}\boldsymbol{\Phi}_{\bar{Y}}^{\mathrm{T}}. \tag{24}$$

The PCA bases can be denoted by

$$\boldsymbol{P} = \boldsymbol{\Phi}_{\bar{Y}}^{\mathrm{T}}\bar{\boldsymbol{Y}} = \boldsymbol{\Phi}_{\bar{Y}}^{\mathrm{T}}(\bar{\boldsymbol{X}} + \boldsymbol{U}) = \boldsymbol{\Phi}_{\bar{Y}}^{\mathrm{T}}\bar{\boldsymbol{X}} + \boldsymbol{\Phi}_{\bar{Y}}^{\mathrm{T}}\boldsymbol{U} = \boldsymbol{P}_{\bar{X}} + \boldsymbol{P}_{U} \tag{25}$$

where $\boldsymbol{P}_{\bar{X}} = \boldsymbol{\Phi}_{\bar{Y}}^{\mathrm{T}}\bar{\boldsymbol{X}}$ and $\boldsymbol{P}_{U} = \boldsymbol{\Phi}_{\bar{Y}}^{\mathrm{T}}\boldsymbol{U}$ respectively.

The signal projection $\boldsymbol{P}_{\bar{X}}$ in the PCA domain can be estimated by the LMMSE criterion as [30] described. By transforming the estimated projection $\hat{\boldsymbol{P}}_{\bar{X}}$ back to the time domain, we can obtain the de-noised result of $\bar{\boldsymbol{Y}}$,

$$\hat{\bar{\boldsymbol{X}}} = \boldsymbol{\Phi}_{\bar{Y}}\hat{\boldsymbol{P}}_{\bar{X}}. \tag{26}$$

Then adding the mean values back to $\hat{\bar{\boldsymbol{X}}}$, we get the de-noised dataset $\hat{\boldsymbol{X}}$.

Once $\hat{\boldsymbol{X}}$ is estimated, the central patch and the pixel in the patch can be extracted. Finally, the de-noised pixel in the dataset will be aggregated to reconstruct the noise-free SAR image.

4. De-noising refinement by guided filter

The original LPG-PCA method can suppress most of the noise. Yet there is still residual noise in the filtered image. To illustrate this problem, in Fig. 2 we add multiplicative noise to the test image "Boat". Fig. 2(a) shows the original image "Boat" and Fig. 2(b) is the noisy version by four-look speckles. Fig. 2(c) is the de-noised image by the original LPG-PCA de-noising procedures and most of the speckles is reduced. Fig. 2(e) is the local amplification of Fig. 2(c).

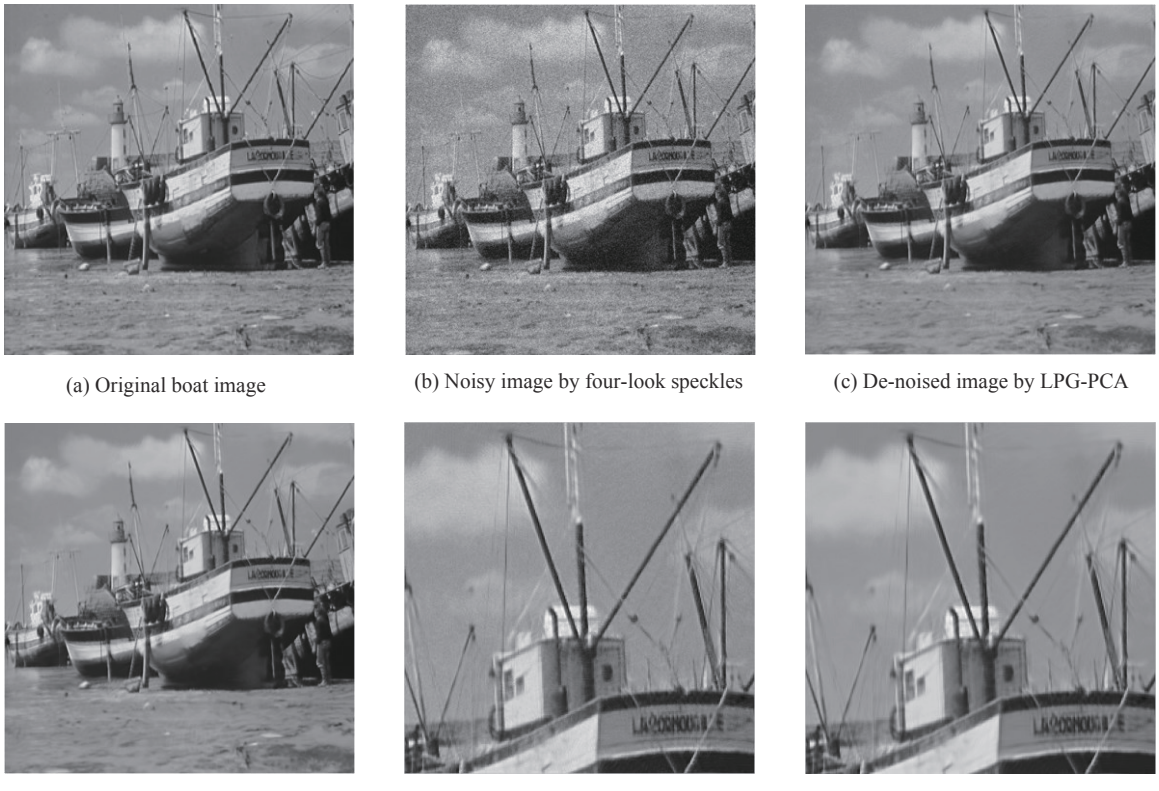

(a) Original boat image (b) Noisy image by four-look speckles (c) De-noised image by LPG-PCA

(d) De-noised image by LPG-PCA and guided filter (e) Local enlargement of Fig. 2(c) (f) Local enlargement of Fig. 2(d)

Fig. 2 Boat image de-noised by the two steps

We can see more clearly that although most of the speckle noise is removed by the LPG-PCA, the noise residue still exists in Fig. 2(e). This is mainly due to the strong speckle noise in SAR images which maybe lead to estimation bias of the PCA transformation matrix. Consequently, we need to further process the LPG-PCA denoising results to achieve a better noise reduction. As a fast non-approximate linear-time method, the guided filter was presented by He et al. in 2013 [31] and updated the fast algorithm in 2015 [32], which can be used as a good edge preserving smoothing method. The guided filter combines the original image and a guidance image to establish a linear filter. The guidance image may be the original input image or another related image. The guided filter can effectively suppress gradient-reversal artifacts. In the following, we refer to the fast guided filter in [32] to update the noise level.

Let $\hat{\boldsymbol{I}}$ be the de-noised version of $\boldsymbol{I}$ in the LPG-PCA denoising algorithm. Naturally, $\hat{\boldsymbol{I}}$ is the input image of the guided filter. Here we also use $\hat{\boldsymbol{I}}$ as the guidance image, and $\boldsymbol{q}$ is the output image. Then the guided filter is driven by a local linear model:

$$\boldsymbol{q}_i = a_k \boldsymbol{I}_i + b_k, \quad \forall i \in \omega_k \tag{27}$$

where i denotes the index of a pixel belonging to a local square window ω_k and k is the index of ω_k. By minimizing the cost function, we can get the linear coefficients:

$$a_k = \frac{\dfrac{1}{|\omega|}\sum_{i\in\omega_k} \boldsymbol{I}_i \hat{\boldsymbol{I}}_i - \mu_k \bar{\hat{\boldsymbol{I}}}_i}{\sigma_k^2 + \varepsilon}, \tag{28}$$

$$b_k = \bar{\hat{\boldsymbol{I}}}_i - a_k \mu_k. \tag{29}$$

where μ_k is the mean and σ_k^2 is the variance of $\boldsymbol{I}$. $\bar{\hat{\boldsymbol{I}}}_i$ and $|\omega|$ denote the mean and the number of pixels in ω_k respectively. Applying (27) to all local windows in the whole image and averaging all the possible values of q_i, we obtain the output data:

$$q_i = \frac{1}{|\omega|}\sum_{k:i\in\omega_k} a_k \boldsymbol{I}_i + b_k = \bar{a}_i \boldsymbol{I}_i + \bar{b}_i \tag{30}$$

where $\bar{a}_i = \dfrac{1}{|\omega|}\sum_{k\in\omega_i} a_k$ and $\bar{b}_i = \dfrac{1}{|\omega|}\sum_{k\in\omega_i} b_k$.

The de-noising results by the LPG-PCA and the guided filter are shown in Fig. 2(d). Fig. 2(f) is the local amplification of Fig. 2(d). We can clearly see that the residual noise is removed greatly after the guided filter.

5. The proposed method

A new SAR image de-noising method based on the LPG-PCA and the guided filter is proposed in this paper. First, we perform logarithm transformation on the multiplicative model to obtain the additive model. Instead of applying the PCA to the original dataset, we suggest using LPG-PCA fitting for SAR images. Although de-noising via the LPG-PCA can suppress the speckle effectively, it also has some error both in the PCA transformation and in LPG because of the strong noise in SAR images. In order to solve this problem, we adopt an improved filtering step in which the output of the LPG-PCA method is filtered by the guided filter. The whole algorithm is presented in Algorithm 1. The detail of the proposed local pixel grouping for SAR images can be seen in Algorithm 2.

Algorithm 1 The proposed SAR images de-noising method.

Input The noisy SAR image $\boldsymbol{I}$.

Step 1 **Coarse filtering.**

Logarithmic transformation with bias correction.

for each pixel $\mathbf{y}_i$ in $\boldsymbol{I}^{(\ln)}$, **do**

Patch extracting. Extract the sliding patches $\mathbf{y}_i$ of size $N\times N$ in the $K\times K$ training block.

Patch grouping. Group the similar patches based on LPG.

De-noising via the PCA.

end for

Obtain the full de-noised image $\hat{\boldsymbol{I}}^{(\ln)}$ of $\boldsymbol{I}^{(\ln)}$.

Exponential transformation. Apply exponential transformation to $\hat{\boldsymbol{I}}^{(\ln)}$ and obtain the coarse filtering result $\hat{\boldsymbol{I}}$.

Step 2 **Improved filtering.**

Initialize Input image $\hat{\boldsymbol{I}}^{(\ln)}$ and guidance image $\boldsymbol{I}$.

Local window ω_k.

Calculate a_k and b_k.

Obtain the de-noised image.

Output The final filtering result $\hat{\boldsymbol{I}}$.

Algorithm 2 The proposed local pixel grouping algorithm for SAR images.

Input The image patches $\boldsymbol{y}_i (i = 1, \cdots, N^{(p)})$

Initialize The training block $K\times K$.

Choose the central patch as the initial patch, denoted by $\boldsymbol{y}_r$.

Let $\boldsymbol{y}_r$ be the current patch and $\boldsymbol{y}_i$ be sample patches around $\boldsymbol{y}_r$ in the training block.

for $i = 1$ to $N^{(p)} - 1$ **do**

Calculate the BSM of $\boldsymbol{y}_r$ and $\boldsymbol{y}_i$ by (18). Choose the patches according to (19) and get the training samples similar to $\boldsymbol{y}_r$.

end for

Output The training set for $\boldsymbol{y}_i$.

6. Experimental results

Without the original noiseless SAR image, it is difficult to make an objective assessment of the method in SAR

image de-noising. Therefore, inspired by [14,15], we add simulated speckle noise to the optical test images and calculate the objective evaluation index. Then in Subsection 6.2, experiments on real SAR images are discussed. We compare the proposed method with several state-of-the-art de-noising methods, such as the Frost filter [3], the homomorphic version of learned simultaneous sparse coding (H-LSSC) [24], original LPG-PCA [30] and nonlocal fast adaptive nonlocal SAR de-noising (FANS) [23].

6.1 Results with simulated speckle

Fig. 3 shows the tested optical images, including House and Cameraman images often used in the AWGN de-noising literature. Furthermore, we choose an "Intersection" image which is more similar to SAR images in the aspect of ground information. The simulated images are obtained by multiplying optical images by simulated white speckle noise with different looks.

(a) House (b) Cameraman (c) Intersection

Fig. 3 Original images used in the experiments

The peak signal-to-noise ratio (PSNR) and structural similarity (SSIM) are used to evaluate the de-noising performance. SSIM was proposed in [33] and often used in the evaluation of despeckling methods. It mainly measures the changes of structure information before and after image filtering.

$$\mathrm{SSIM}=\frac{1}{M}\sum_{p=0}^{M-1}\frac{2\mathrm{E}[\boldsymbol{I}_p]\cdot\mathrm{E}[\hat{\boldsymbol{I}}_p]+C_1}{\mathrm{E}[\boldsymbol{I}_p^2]+\mathrm{E}[\hat{\boldsymbol{I}}_p^2]+C_1}\cdot\frac{2\mathrm{cov}[\boldsymbol{I}_p,\hat{\boldsymbol{I}}_p]+C_2}{\mathrm{Var}[\boldsymbol{I}_p]+\mathrm{Var}[\hat{\boldsymbol{I}}_p]+C_2} \tag{31}$$

where $\boldsymbol{I}_p$ and $\hat{\boldsymbol{I}}_p$ represent noise-free image patches and de-noised image patches respectively. C_1 and C_2 denote constants that are not zero. SSIM is a number greater than 0 and less than 1. The closer SSIM is to 1, the more similar the structure is.

Table 1 shows the PSNR of different realizations of the noise process. As can be seen from Table 1, the PSNR by our method is similar to FANS and much better than the other methods. Especially when L is smaller, the value of PSNR by the proposed method is about 5 dB larger than that of the H-LSSC. This is mainly due to lots of irrelevant patches in the learned dictionary which are not helpful for sparse representation. The SSIM indices by different methods are shown in Table 2. We can see that the SSIM indices obtained by our method is optimal.

Table 1 PSNR results of the de-noised image by different methods dB

Method	House				Cameraman				Intersection			
	L=1	L=2	L=4	L=16	L=1	L=2	L=4	L=16	L=1	L=2	L=4	L=16
Noisy	11.28	13.15	16.34	22.56	12.23	15.12	18.45	24.32	11.12	16.81	22.76	24.96
Frost	18.23	21.48	25.56	29.67	19.56	22.34	26.78	29.89	20.67	21.89	24.78	27.45
H-LSSC	22.23	22.71	26.89	32.54	22.91	25.54	27.90	32.98	20.71	23.94	26.29	28.89
LPG-PCA	26.85	25.03	28.56	34.16	28.08	30.45	30.01	33.91	21.45	24.83	26.12	29.03
FANS	26.91	28.72	33.31	34.28	30.01	30.90	33.19	35.76	21.91	26.06	27.98	29.92
The proposed method	28.14	29.12	33.45	34.25	29.70	31.24	34.59	34.78	25.28	26.98	27.90	29.99

Due to the limitation of space, only partial de-noising results are shown in this paper. Fig. 4 shows the de-noised images by different methods for the "Intersection" image with L=2. From the de-noised images in Fig. 4, we

notice that the Frost filter cannot remove all of the speckle noise. H-LSSC keeps working very well on the homogeneous region while unsatisfactory on the heterogeneous region. The original LPG-PCA method de-noises the log-transformed data directly which is not suitable for SAR speckle noise and produces many dark artifacts. Our method considers the multiplicative properties of speckle noise and uses the ad hoc BSM based on the real speckle noise distribution which greatly outperforms the original LPG-PCA on different looks. From Fig. 4, we can see that both FANS and the proposed method can suppress speckle noise without destroying boundary information while the proposed method produces fewer artifacts.

Table 2 SSIM results for "Intersection"

Method	L=1	L=2	L=4	L=16
Noisy	0.657 8	0.732 3	0.852 3	0.902 1
Frost	0.686 7	0.753 4	0.903 4	0.910 9
H-LSSC	0.711 3	0.824 5	0.908 5	0.949 5
LPG-PCA	0.712 3	0.892 3	0.932 3	0.967 8
FANS	0.789 8	0.903 1	0.930 9	0.989 1
Proposed method	0.790 2	0.908 1	0.940 1	0.989 8

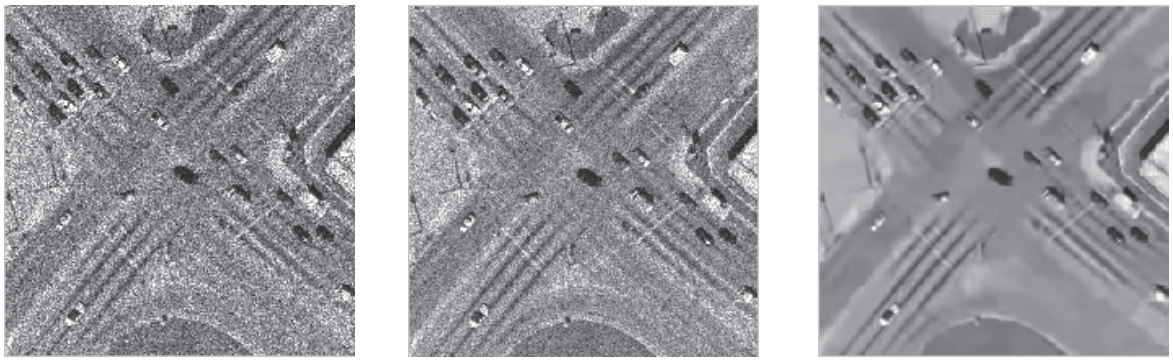

(a) Noisy image (b) Frost (c) H-LSSC

(d) LPG-PCA (e) FANS (f) The proposed method

Fig. 4 De-noised images for "Intersection" corrupted by two-look speckles

6.2 Results with real SAR images

In order to further verify the effectiveness of the proposed method, comparison experiments of different methods on the real SAR images taken by TerraSAR-X over Swabian Jura (SJ) in Germany and Black Rock City (BRC) in USA are shown in Fig. 5 and Fig. 6. As we know, the ENLs is a standard parameter widely used in the remote sensing. It can measure the ability to suppress the noise in homogeneous areas. The white boxes in Fig. 5(a) and Fig. 6(a) are used to compute the ENLs. Larger ENLs values indicate stronger speckle suppression and an improved ability to distinguish different gray levels. From the ENLs results in Table 3, we can find that the proposed method has excellent ENLs in homogeneous areas.

From Fig. 5 and Fig. 6, we can find that Frost still remains much noise in both homogeneous and heterogeneous areas. H-LSSC may over-smooth the whole area. All methods preserve well on the linear structures expect for some lost in H-LSSC. The original LPG-PCA pro-

duces some artifacts because of the unsuitable grouping. The proposed method outperforms FANS in terms of small details preservation especially in heterogeneous areas.Overall, it shows that the proposed method is better than the other referenced methods in terms of both simulated images and real SAR images.

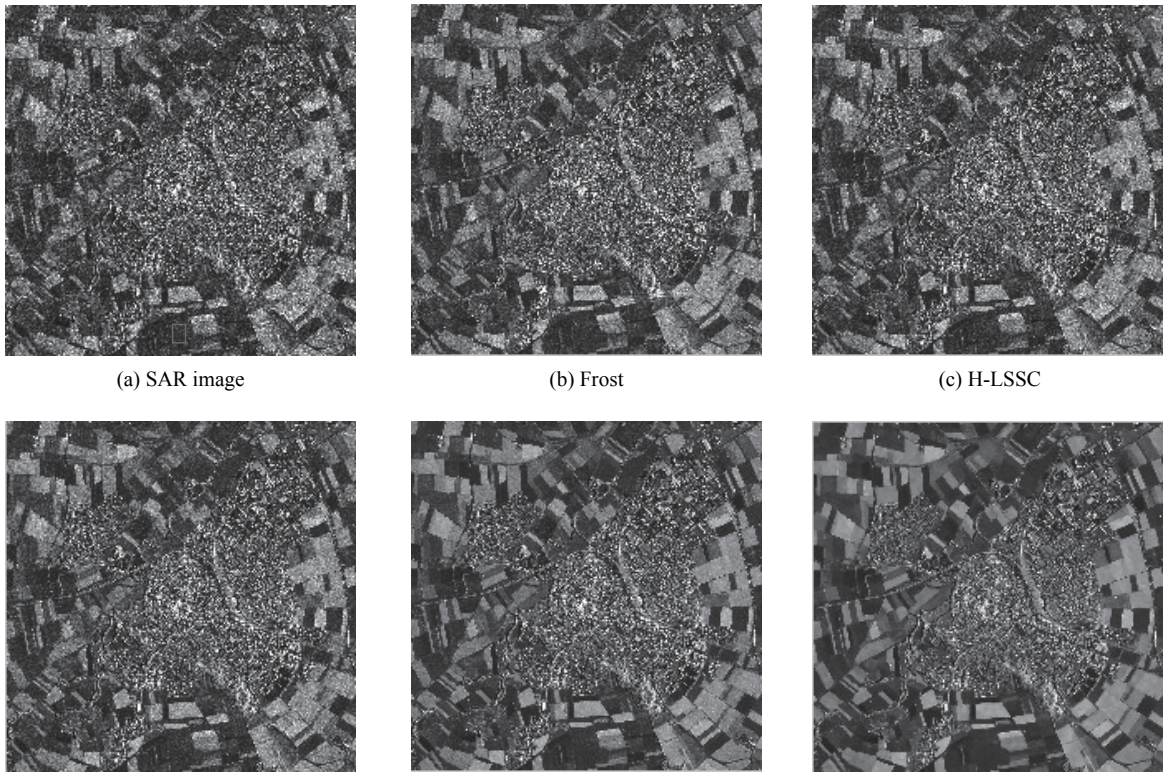

(a) SAR image (b) Frost (c) H-LSSC

(d) LPG-PCA (e) FANS (f) The proposed method

Fig. 5 De-noised images for SJ

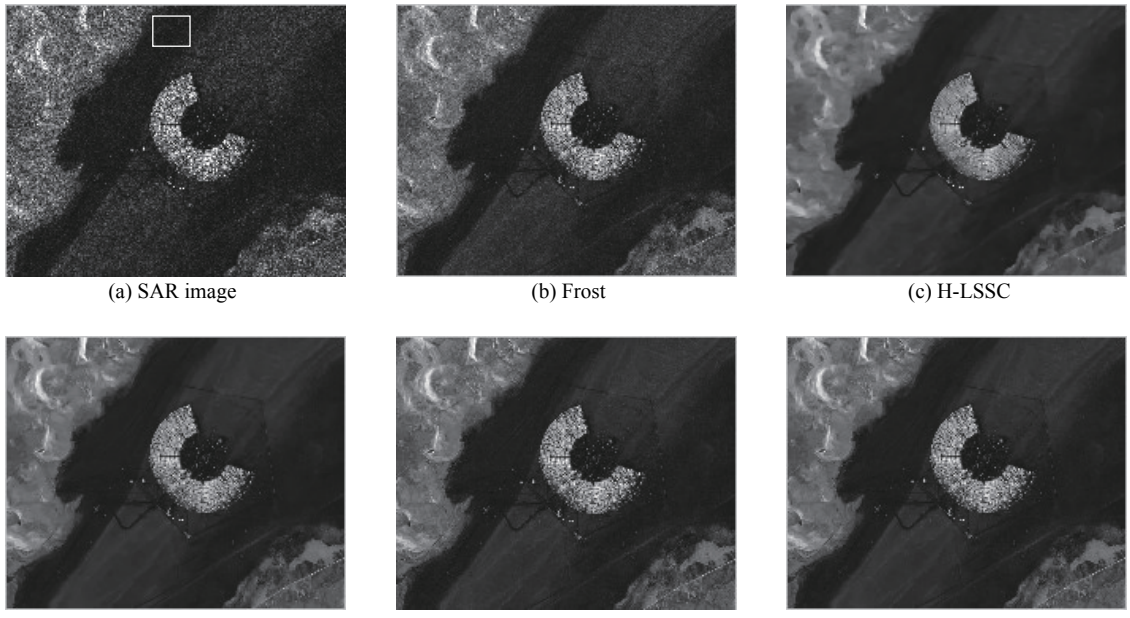

(a) SAR image (b) Frost (c) H-LSSC

(d) LPG-PCA (e) FANS (f) The proposed method

Fig. 6 De-noised images for BRC

Table 3 ENLs for real SAR images

Method	SJ	BRC
Noisy	7.56	0.91
Frost	9.09	2.56
H-LSSC	14.61	3.67
LPG-PCA	11.23	6.87
FANS	12.78	7.93
The proposed method	13.14	8.04

7. Conclusions and future work

A spatially adaptive image de-noising method by using the LPG-PCA and the guided filter is proposed in this paper. Compared with the state-of-the-art SAR image de-noising methods, the proposed method achieves a better performance in terms of PSNR and SSIM by the experiment on simulated images. Besides, our method has better visual effects and shows fewer artifacts. For real SAR images, the ENLs is used to evaluate the ability of noise suppression in homogeneous areas. The proposed method has a very strong noise reduction ability while preserving the detail better.

Different from ordinary optical images, there are much texture information and edge features in SAR images. A certain point in SAR images may correspond to a building on the ground. The isolated structures have almost no similar patches in the search area which may lead to inaccurate estimation of the covariance matrix. Future research will concentrate on the separation of the isolated structures and perform different de-noising methods in different areas.

References

[1] MOREIRA A, PRATS-IRAOLA P, YOUNIS M, et al. A tutorial on synthetic aperture radar. IEEE Geoscience Remote and Sensing Magazine, 2013, 1(1): 6–43.

[2] GOODMAN J W. Some fundamental properties of speckle. Journal of the Optical Society of America, 1976, 6(11): 1145–l150.

[3] FROST V S, STILES J A, SHANMUGAN K S, et al. A model for radar images and its application to adaptive digital filtering of multiplicative noise. IEEE Trans. on Pattern Analysis and Machine Intelligence, 1982, 4(2): 157–166.

[4] FROST V S, SHANMUGAN K S. The information content of synthetic aperture radar images. IEEE Trans. on Aerospace and Electronic Systems, 1983, 19(5): 768–774.

[5] ARSENAULT H H, LEVESQUE M. Combined homomorphic and local statistics processing for restoration of images degraded by signal dependent noise. Applied Optics, 1984, 23(6): 845–850.

[6] YAN P F, CHEN C H. An algorithm for filtering multiplicative noise in wide range. Traitement du Signal, 1986, 3(2): 91–96. (in French)

[7] ARSENAULT H H, APRIL G. Properties of speckle integrated with a finite aperture and logarithmically transformed. Journal of the Optical Society of America, 1976, 66(11): 1160–1163.

[8] LEE J S. Digital image enhancement and noise filtering by use of local statistics. IEEE Trans. on Pattern Analysis and Machine Intelligence, 1980, 2(2): 165–168.

[9] LEE J S. Refined filtering of image noise using local statistics. Computer Graphics and Image Processing, 1981, 15(4): 380–389.

[10] KUAN D T, SAWCHUK A A, STRAND T C, et al. Adaptive noise smoothing filter for images with signal-dependent noise. IEEE Trans. on Pattern Analysis and Machine Intelligence, 1985, 7(2): 165–177.

[11] LOPES A, TOUZI R, NEZRY E. Adaptive speckle filters and scene heterogeneity. IEEE Trans. on Geoscience and Remote Sensing, 1990, 28(6): 992–1000.

[12] GUO H, ODEGARD J, LANG M, et al. Wavelet based speckle reduction with application to SAR based ATD/R. Proc. of the IEEE International Conference on Image Processing, 1994: 75–79.

[13] ACHIM A, TSAKALIDES P, BEZARIANOS A. SAR image de-noising via Bayesian wavelet shrinkage based on heavy-tailed modeling. IEEE Trans. on Geoscience and Remote Sensing, 2003, 41(8): 1773–1784.

[14] BHUIYAN M, AHMAD M, SWAMY M. Spatially adaptive wavelet based method using the Cauchy prior for de-noising the SAR images. IEEE Trans. on Circuits and Systems for Video Technology, 2007, 17(4): 500–507.

[15] XIE H, PIERCE L, ULABY F. Despeckling SAR images using a low complexity wavelet de-noising process. Proc. of the IEEE International Geoscience and Remote Sensing Symposium, 2002: 321–324.

[16] ARGENTI F, ALPARONE A. Speckle removal from SAR images in the undecimated wavelet domain. IEEE Trans. on Geoscience and Remote Sensing, 2002, 40(11): 2363–2374.

[17] COUPE P, HELLIER P, KERVRANN C, et al. Bayesian non local means-based speckle filtering. Proc. of the IEEE International Symposium on Biomedical Imaging: from Nano to Macro, 2008: 1291–1294.

[18] DELEDALLE C, DENIS L, TUPIN F. Iterative weighted maximum likelihood de-noising with probabilistic patch-based weights. IEEE Trans. on Image Processing, 2009, 18(12): 2661–2672.

[19] PARRILLI S, PODERICO M, ANGELINO C, et al. A nonlocal approach for SAR image de-noising. Proc. of the Geoscience and Remote Sensing Symposium, 2010, 45(1): 726–729.

[20] ZHONG H, XU J, JIAO L C. Classification based nonlocal means despeckling for SAR image. Proceedings of SPIE — The International Society for Optical Engineering, 2009. DOI: 10.1117/12.832169.

[21] PARRILLI S, PODERICO M, ANGELINO C V, et al. A nonlocal SAR image de-noising algorithm based on LLMMSE wavelet shrinkage. IEEE Trans. on Geoscience and Remote Sensing, 2012, 50(2): 606–616.

[22] TORRES L, FRERY A C. SAR image despeckling algo-

rithms using stochastic distances and nonlocal means, 2013, http://arxiv.org/abs/1308.4388?context=stat^ML.
[23] COZZOLINO D, PARRILLI S, SCARPA G, et al. Fast adaptive nonlocal SAR despeckling. IEEE Geoscience and Remote Sensing Letters, 2014, 11(2): 524–528.
[24] CHIERCHIA G, El GHECHE M, SCARPA G, et al. Multitemporal SAR image despeckling based on block-matching and collaborative filtering. IEEE Trans. on Geoscience and Remote Sensing, 2017, 55(10): 1–14.
[25] WANG P Y, ZHANG H, PATEL V M. SAR image despeckling using a convolutional neural network. IEEE Signal Processing Letters, 2017, 24(12): 1763–1767.
[26] FERRAIOLI G, PASCAZIO V, VITALE S. A novel cost function for despeckling using convolutional neural networks. Joint Urban Remote Sensing Event, 2019. DOI: 10.1109/JURSE.2019.8809042.
[27] FUKUNAGA K. Introduction to statistical pattern recognition. 2nd ed. New York: Academic Press, 1991.
[28] FANG J, LIU S Q, XIAO Y, et al. SAR image de-noising based on texture strength and weighted nuclear norm minimization. Journal of Systems Engineering and Electronics, 2016, 27(4): 807–814.
[29] MURESAN D D, PARKS T W. Adaptive principal components and image de-noising. Proc. of the IEEE International Conference on Image Processing, 2003: 101–104.
[30] ZHANG L, DONG W S, ZHANG D, et al. Two-stage image de-noising by principal component analysis with local pixel grouping. Pattern Recognition, 2010, 43(4): 1531–1549.
[31] HE K M, SUN J, TANG X O. Guided image filter. IEEE Trans. on Pattern Analysis and Machine Intelligence, 2013, 35(6): 1397–1409.
[32] HE K M, SUN J. Fast guided filter. Computer Science, 2015, htttp://arxiv.org/abs/1505.00996.
[33] WANG Z, BOVIK A C, SHEIKH H R, et al. Image quality assessment: from error visibility to structural similarity. IEEE Trans. on Image Processing, 2004, 13(4): 600–612.

Biographies

FANG Jing was born in 1980. She received her M.S. and Ph.D. degrees in Institute of Information Science from Beijing Jiaotong University, in 2005 and 2020, respectively. She has been a lecturer in Shandong Normal University since 2008. She has co-authored more than 15 journal articles and conference proceedings. Her research interests include SAR image processing and signal processing.
E-mail: fangjing@sdnu.edu.cn

HU Shaohai was born in 1964. He received his B.S. and M.S. degrees in the Department of Electronic Engineering from Beihang University in 1985 and 1988, respectively. He received his Ph.D. degree in Institute of Information Science from Beijing Jiaotong University in 1991 and has been a professor of Institute of Information Science since 2008. He has co-authored more than 100 journal articles and conference proceedings, and has published three books in his research area. His research interests include signal processing and information fusion, including image fusion, image denosing and sparse representation.
E-mail: shhu@bjtu.edu.cn

MA Xiaole was born in 1991. She received her B.S. degree in communication engineering at Electronic Information Engineering from Hebei University in 2015, and Ph.D. degree in Institute of Information Science from Beijing Jiaotong University in 2020. She had been a visiting scholar at University of Missouri-Columbia from 2018 to 2019. Currently, she is a postdoctoral fellow in Institute of Information Science from Beijing Jiaotong University. Her research interests include image fusion and sparse representation.
E-mail: maxiaole@bjtu.edu.cn